Distribution Agreement:

In presenting this thesis as a partial fulfillment of the requirements for a degree from Emory University, I hereby grant to Emory University and its agents the non-exclusive license to archive, make accessible, and display my thesis in whole or in part in all forms of media, now or hereafter known, including display on the world wide web. I understand that I may select some access restrictions as part of the online submission of this thesis. I retain all ownership rights to the copyright of the thesis. I also retain the right to use in future works (such as articles or books) all or part of this thesis.

Signature:

Ruth Blum	April 18, 2010

Numerical Simulations of Aortic Blood Flow with a Bicuspid Aortic Valve

By

Ruth D. Blum

Advisor Alessandro Veneziani

Department of Mathematics and Computer Science

_____

Alessandro Veneziani
Advisor

_____

Michele Benzi
Committee Member

_____

David Borthwick
Committee Member

_____

Jonathan Master
Committee Member

_____

April 18, 2010

Numerical Simulations of Aortic Blood Flow with a Bicuspid Aortic Valve

By

Ruth D. Blum

Advisor Alessandro Veneziani

An abstract of
A thesis submitted to the Faculty of Emory College of Arts and Sciences of
Emory University in partial fulfillment of the requirements of the degree of
Bachelor of Sciences with Honors

Department of Mathematics and Computer Science

2010

Abstract

Numerical Simulations of Aortic Blood Flow with a Bicuspid Aortic Valve
By Ruth D. Blum

One of the most common congenital heart defects is bicuspid aortic valve (BAV), occurring in about 1% to 2% of the population. In patients with BAV the aortic valve deviates from normal in that it only has two leaflets instead of three. BAV can result in altered hemodynamics and decreased performance of the valve, which in turn can lead to serious complications, such as aortic dilation, stenosis, regurgitation, aneurysms, dissection and infective endocarditis. This research focuses on understanding the pathology behind one complication associated with bicuspid aortic valves in particular: *aortic dilation*. This is primarily because aortic dilation is correlated to greatly increased risk for further complications such as aortic regurgitation, formation of an aortic aneurysm or aortic dissection.

The framework to which the present work belongs is a project for investigating the fluid dynamics in the ascending aorta of patients with BAV in order to reveal the hemodynamic mechanisms possibly causing aortic dilation in some patients and not others. Differences in bicuspid aortic valve morphologies due to the fusion of different combinations of cusps and different inlet sizes were considered, and an idealized geometry of the aorta was used. This investigation was conducted via three-dimensional computational models that are able to provide reliable evaluation of various hemodynamic and anatomical parameters, relevant for prediction and quantification of aortic dilation.

It was found that as the size of the inlet decreases, the velocity, pressure and wall shear stress all increase in the ascending aorta. Blood vessel wall remodeling is associated with prolonged increases of pressure and flow rate, and so narrow inlets may be correlated with aortic dilation. It is unclear how the fusion of different leaflets is correlated with pathologies of the aortic arch, but when coupled with a small inlet, rotated inlets induce asymmetry of the blood flow. At this point in the research it can be concluded that there is something inherent with blood flow in the aortic arch in models with bicuspid aortic valves that is intrinsically different from the normal tricuspid aortic valve flow. Additionally, this flow differs depending on the specific morphology of the bicuspid aortic valve under investigation.

Numerical Simulations of Aortic Blood Flow with a Bicuspid Aortic Valve

By

Ruth D. Blum

Advisor Alessandro Veneziani

A thesis submitted to the Faculty of Emory College of Arts and Sciences of Emory University in partial fulfillment of the requirements of the degree of Bachelor of Sciences with Honors

Department of Mathematics and Computer Science

2010

Acknowledgements

I would like to acknowledge Tiziano Passerini who acted as a co-advisor on this research project and spent many hours teaching and mentoring me throughout this year. I would like to thank Michele Benzi, David Borthwick and Jonathan Master for their comments on the work, and for being such great professors. I would also like to thank the Emory Mathematics and Computer Science department as a whole for expanding my knowledge and love of mathematics and for making my time at Emory at great one. Lastly, I would like to thank my parents, for without their endless encouragement and support none of this would have been possible.

CONTENTS

ILLUSTRATIONS

Figures

Equations

1. Introduction

1.1 Background

In a normally functioning human heart, oxygenated blood is pumped from the left ventricle through the aortic valve and into the aorta, the major systemic artery. The aortic valve serves to prevent blood ejected from the left ventricle from regurgitating back into the ventricle itself [1]. In a normal heart, the aortic valve is "tricuspid," consisting of three relatively symmetric leaflets or "cusps" (Figure 1.1). These leaflets are named for their proximity to the location where the left and right coronary arteries originate from the aorta, just distal to the valve, and are thus often referred to as the *left-, right- and non-coronary* cusps [2]. When the valve is closed, the three leaflets come together, providing mutual support [3].

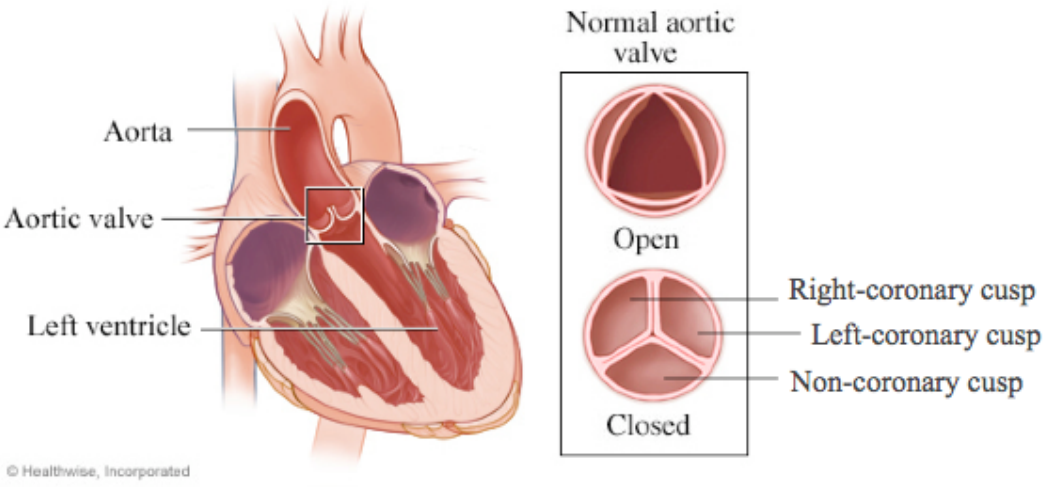

Figure 1.1 A normal aortic valve [1].

However, not everyone's aortic valve develops normally. The most common congenital heart defect is bicuspid aortic valve (BAV), occurring in about 1% to 2% of the population [4]. In patients with bicuspid aortic valve the aortic valve

deviates from normal in that it only has two leaflets instead of three. The appearance is often described as two of the leaflets being "fused" (figure 1.2). Bicuspid aortic valve can result in altered hemodynamics and decreased performance of the valve, which in turn can lead to serious complications.

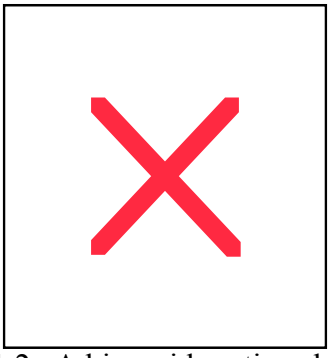

Figure 1.2 A bicuspid aortic valve [5].

1.2 Significance

The study of the altered blood flow and flow dynamics due to the morphology of bicuspid aortic valves is important in understanding the pathology of the complications caused by the defect. These serious complications occur in at least one third of patients with bicuspid aortic valves and may include aortic dilation, aortic stenosis, aortic regurgitation, infective endocarditis, aortic aneurysms or aortic dissection [6, 7]. Considering that congenital bicuspid aortic valves occur in about 1% - 2% of the population, at least one third of which develop serious complications, and that all other forms of congenital heart disease are thought to be present in only 0.8% of live births, it is suggested that bicuspid aortic valves are likely to result in more morbidity and higher mortality than all other congenital heart defects combined [7]. Understanding the mechanisms that lead

to these complications could help reduce the morbidity and mortality associated with bicuspid aortic valves by eventually leading to better health management protocols and treatment.

This research focuses on understanding the pathology behind one complication associated with bicuspid aortic valves in particular: *aortic dilation*. This is primarily because aortic dilation is correlated to greatly increased risk for further complications such as aortic regurgitation, formation of an aortic aneurysm or aortic dissection [6]. Aortic dilation develops at a young age, as determined by Nistri, who conducted a study and found that at a mean age of 17.8 years, 52% of males with 'normally' functioning bicuspid aortic valves have already developed aortic dilation [6]. It is worth noting that a *normally functioning* bicuspid aortic valve is typically defined as one that functions with the absence of significant valve regurgitation or aortic stenosis, both of which are usually considered early complications of bicuspid aortic valves and precursors for further complications. Therefore, Nistri's findings imply that valve function problems such as regurgitation and aortic stenosis are not obligate precursors for other complications, like aortic dilation, as once thought.

Despite Nistri's study, clinicians have not focused much attention on normally functioning bicuspid aortic valves in young patients, since many patients do not develop significant problems until well into adulthood. However, there is immediate clinical significance to the study as patients with a dilated aorta have a 9-fold increased risk of aortic dissection [7, 8] and have an increased risk of

sudden cardiac death, even after valve replacement [9, 10, 11], and as of now there are no reliable methods for predicting aortic dilation.

Therefore, the framework to which the present work belongs is a project for investigating the fluid dynamics in the ascending aorta of patients with bicuspid aortic valves in order to reveal the hemodynamic mechanisms possibly causing aortic dilation in some patients and not others. If reliable prediction methods for the development of aortic dilation can be developed, then that would enable risk stratification, which may allow the establishment of more individualized management protocols for patients. This could include following low-risk patients with relatively infrequent evaluations, but following high-risk patients with more aggressive clinical strategies, such as treating them with new or existing medications in order to prevent aortic dilation. Improved management protocols for patients with bicuspid aortic valves has the potential to decrease the need for surgical replacement of dilated ascending aortas and/or aortic valves and to reduce the risk of other serious complications such as aortic aneurysms, dissections or rupture.

1.3 Prior Studies

There have been several previous studies that have demonstrated an association between bicuspid aortic valves and dilation of the aorta [4, 6, 12, 13, 14]. As mentioned earlier, Nistri et al. found a correlation between young men with bicuspid aortic valves and aortic dilation. Another study was conducted by Gurvitz et al, who performed echocardiography measurements in children and

found that those with bicuspid aortic valves had significantly larger aortic roots than the healthy subjects regardless of the presence of stenosis or regurgitation [13]. However, despite these findings, it still remains unclear from the literature whether aortic dilation is secondary to abnormal blood flow patterns and associated increased forces, pressures and shear stresses operating on the aortic wall due to a particular bicuspid aortic valve morphology, or vice versa. That is, whether dilation actually is caused by altered blood flow patterns or whether it is a manifestation of a distinct underlying structural problem with not only the aortic valve but also the aortic root including the ascending aorta [15, 16, 17]. For example, Fedak et al. suggest that aortic dilation might be the result of a defect in vascular matrix remodeling, which might be due to altered gene expression of microfibrillar proteins and their assembly into stable matrix components [16]. However, Fedak's studies are inconclusive at this time.

Another aspect of bicuspid aortic valves that has to be considered is the particular differences in their morphology. For instance, the two leaflets may be similar in size, creating a symmetric inlet, or differ in size, creating an asymmetric inlet. Also, differences in the cusps that are fused may create different inlet angles. These differences in morphologies may result in different pathologies. For example, Fernandes et al. reviewed the echocardiographs of 1,135 children with bicuspid aortic valves and found differences among the pathologies of the patients related to aortic valve morphology [18]. For instance, 9.7% of patients with fusion of the left-coronary and right-coronary cusps of the aortic valve experienced moderate or greater aortic stenosis, versus 25.9% of patients with

fusion of the right-coronary and non-coronary cusps. Additionally, fusion of the right-coronary and non-coronary cusps resulted in a two-fold higher risk of at least moderate aortic regurgitation compared with the other morphologies of bicuspid aortic valves. However, Fernandes et al. did not report on whether there was any relationship between valve morphology and aortic root dilation. Holmes et al. conducted a study where 112 pediatric patients (mean age of 8.5 years) with bicuspid aortic valves with echocardiographic exams were reviewed and found on univariate analysis that fusion of the right-coronary and non-coronary cusps was associated with aortic dilation [14]. However, on multivariate analysis, this finding did not reach clinical significance. Novaro et al. also conducted a study where they found that adult patients (mean age of 54 years) with fusion of the right-coronary and non-coronary cusps tended to have larger mid-ascending aortas than patients with fusion of the right-coronary and left-coronary cusps, but this finding again did not reach statistical significance [19]. Despite the lack of statistically significant evidence correlating different bicuspid aortic valve morphologies with differences in aortic dilation, recent publications support the assertion that individual bicuspid aortic valves may function quite differently from one another, and so it is definitely worth investigating further.

1.4 Summary

The objective of this research project is to improve the understanding of the hemodynamic mechanisms that possibly contribute to aortic dilation in patients with bicuspid aortic valves. Differences in bicuspid aortic valve morphologies due

to the fusion of different combinations of cusps will be considered, and a symmetric inlet will be assumed, meaning that the two leaflets are the same size and shape. It is hypothesized that the early risk stratification of bicuspid aortic valve patients can be accomplished through visual and quantitative analysis of altered blood flow due to the morphology and flow dynamics associated with the bicuspid valve. According to the considered underlying model, blood flow jets directed at the aortic wall are associated with increased local pressure and shear stress, resulting in aortic wall remodeling and accelerated aortic dilation [15, 16]. This is due to the fact that blood vessels often structurally change in response to prolonged increases of pressure or flow rate [3]. This investigation will be conducted by three-dimensional computational models that are able to provide reliable evaluation of various hemodynamic and anatomical parameters, relevant for prediction and quantification of aortic dilation.

In the following sections there will be a detailed description of the development of the mathematical model and the numerical simulations performed using the model. The results will then be interpreted using visualization software and explained in detail. Finally, the results will be discussed and conclusions will be drawn in an attempt to find a correlation between the results and the development of pathologies in the aortic arch in patients with bicuspid aortic valve.

2. Methods

2.1 Computational Fluid Dynamics

The use of computational fluid dynamics (CFD) in investigating the physiopathology of the cardiovascular system has only become widespread within the bioengineering and medical research community in the past few decades [3]. The main reasons for the increased popularity of CFD as a well-established research tool are advancements in the power of modern computers, the progress of 3-D high-resolution medical imaging tools (in particular MRI and CT angiographic techniques) and image processing methods for the reconstruction of vascular geometry, as well as the development of better numerical algorithms for the efficient solution of the fluid dynamics problem [3]. In fact, many recent developments in basic computational fluid dynamics methodologies have been motivated by the study of hemodynamics and its applications. Much of the research done thus far has focused on simulating biochemical and mechanical interactions between blood and the vascular walls, as well as on methods for the simulation of both local and systemic dynamics of the vascular system [20, 21].

There are several advantages in using CFD to characterize the cardiovascular system (sometimes called *in silico* models), instead of more traditional *in vivo* or *in vitro* experimental studies:

a) the relatively low costs associated with *in silico* models.
b) The less invasive nature of numerical simulations, since only minimal measurements from the patient are needed [3].

c) The ability to precisely control boundary conditions set in the models.

d) The ability to accurately compute quantities that are difficult or impossible to measure *in vivo*, such as local wall pressure and wall shear stress.

Comparing the numerical results to patient specific measurements can validate the CFD model. If the matching is satisfactory, then the model can be used with confidence to extract other information on the system. In the case of patients with bicuspid aortic valve, an additional strength of computational fluid dynamics can be exploited: the ability to evaluate several different anatomical and functional configurations, studying separately the effect of different parameters on the resulting hemodynamic environment.

The core part of CFD modeling is the numerical solution of the mathematical equations constituting the adopted physical model for blood flow. Usually, these are partial differential equations. This task requires some data from the patient, which usually includes the value of parameters characterizing the blood and vessel walls (such as the mass density), initial conditions and boundary conditions necessary for solving the partial differential equations and geometrical data so that the shape of the computational domain can be accurately defined [3]. A generic procedure for computational fluid dynamic modeling of blood flow is as follows:

1. acquire medical images of the desired cardiovascular area from CT, MRI, angiographic imaging, etc [22].
2. Reconstruct a 3-D geometric model of the individual vascular surface inside which blood flow simulations can be carried out [23, 24, 25]. Note

that in some cases the wall thickness is reconstructed as well in order to obtain information about the mechanical properties of the wall.

3. Prescribe proper boundary conditions for the blood flow possibly based on measurements or systemic models [26, 27, 28, 29].
4. Perform the appropriate numerical simulation, by solving the underlying equations.
5. Interpret the data by using post-processing techniques.

This basic methodology can be used to model blood flow in the aorta of patients with bicuspid aortic valves; the details of how this procedure will be applied to the objectives of this investigation will be discussed in the following sections.

2.2 Starting Assumptions

Blood is a complex mixture, consisting of a suspension of particles in the plasma, which mostly consists of water. Red blood cells are the principal type of particle found in the plasma. Therefore, they contribute the most to the mechanical properties of blood, the most prominent of which is that blood is a *shear-thinning fluid*. In the simplest terms this means that the more blood is stirred, the more it fluidifies, that is, its viscosity decreases the more it is agitated [3]. However, in larger vessels, such as the aorta, the shear-thinning and viscoelastic effects of blood are negligible and may be ignored [3]. In these cases, blood may be assumed to have a constant viscosity, meaning it behaves as a Newtonian fluid. This assumption will be exploited in the following since the physical region that is being investigated is a small region of the aorta, starting at

the junction with the left ventricle, which is where most complications of bicuspid aortic valve occur.

It is challenging to numerically model the movement of the aortic valve. Capturing its fast dynamics requires a great computational effort, especially when considering the coupled fluid-structure interaction problem of the thin structure of the valve embedded into the blood flow [30]. A remarkable contribution in this field, the so-called Immersed Boundary Method, has been given by C. Peskin, but the computational complexity to be faced in this case is out of the scope of the present work [31].

Moreover, it is worth pointing out that two arguments strongly support the choice of neglecting the vascular wall movement in the computational fluid dynamic model. On the one hand, an accurate and validated mechanical model would be required for the description of the vessel movement during the cardiac cycle. There is debate in the literature on the validity of currently proposed models for this purpose [32]. Moreover, they typically require additional data for the mechanical characterization of the biological tissue or wall displacement measures, which are seldom available. On the other hand, the assumption of rigid wall geometry is commonly accepted in computational hemodynamics, especially when the focus of the study is the comparison of blood flow features in different experimental setup [3].

For these reasons, simulations will consider only the region *downstream* of the valve and the effects of the shape of the aortic valve will be taken into account by the boundary conditions of the fluid. Simulations will be performed in rigid

geometries and the geometry will have relatively "average" features and dimensions. A simplified "candy-cane" shape will be used, with the radius of the aorta and aortic arch prescribed as 1.5 cm and 6.0 cm respectively. The aim of this project is indeed to qualitatively evaluate the effects of different boundary conditions (representing different manifestation of the bicuspid aortic valve disease) on the fluid dynamics of blood in an idealized geometry of the aortic arch.

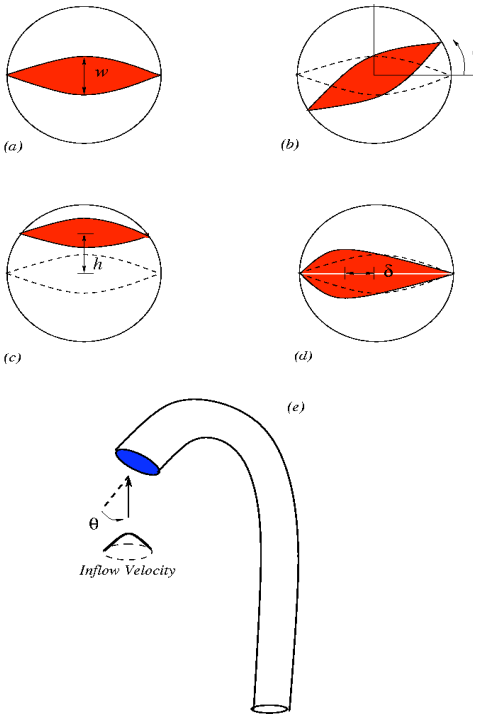

Figure 2.1 Five degrees of freedom for the inlet conditions.
(a) Size *w* of the effective inlet section (in red),
(b) Rotation angle α of the effective inlet section,
(c) Vertical offset *h,*
(d) Horizontal offset δ of the maximum opening of the section,
(e) Angle θ of inflow velocity with respect to the orientation of the inflow section.

Five different degrees of freedom for the inlet conditions can be considered as seen in figure 2.1, but in this investigation only the size *w* of the inlet section and the rotation angle α of the inlet section will be varied. Regarding the other three degrees of freedom, the inlet section is assumed to be centered (h=0) and

symmetric ($\delta=0$), and the angle θ of the inflow velocity with respect to the normal vector to the inflow section is assumed to be 0^{o}.

There will be three different rotation angles and three different inlet widths considered. The angle of the inlet is dependent on the fusion of the leaflets, for which there are several possibilities. Lerer and Edwards conducted a study on 50 patients with bicuspid aortic valves and found that the right-coronary and left-coronary leaflets were fused in 72% of the patients, the right-coronary and non-coronary leaflets were fused in 26% of the patients and the left-coronary and non-coronary leaflets were fused in 2% of the patients [33], as can be seen below in figure 2.2.

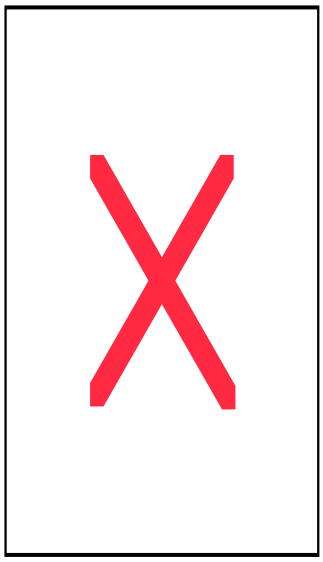

Figure 2.2 Illustration of the three different possible leaflet fusions. *(a)* Fusion of the right-coronary and non-coronary leaflets. *(b)* Fusion of the right-coronary and non-coronary leaflets. *(c)* Fusion of the left-coronary and non-coronary leaflets [33].

From hereafter, the angle corresponding to the fusion of the right-coronary and left-coronary leaflets, the right-coronary and non-coronary leaflets and the left-coronary and non-coronary leaflets will be 90, 45, and 135 degrees, respectively (figure 2.3).

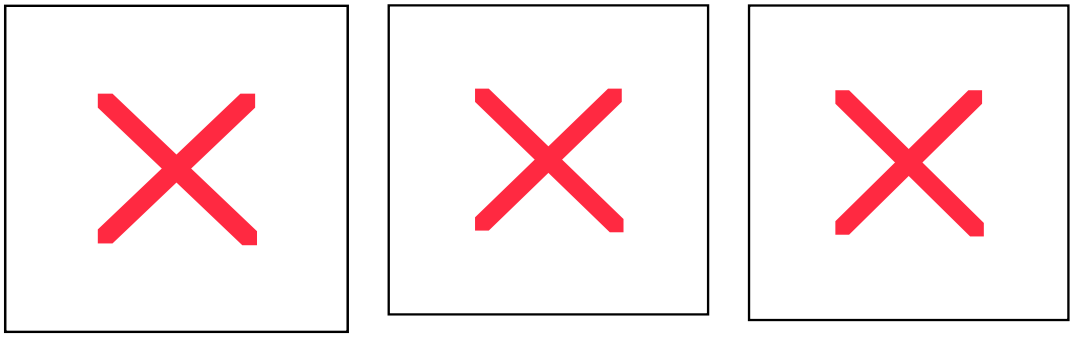

Figure 2.3 Inlet rotation angles used to describe the different fusions of leaflets. *(a)* Fusion of the right- and left- coronary leaflets ($\alpha = 90^{o}$), *(b)* fusion of the left- and non-coronary leaflets ($\alpha = 45^{o}$), *(c)* fusion of the right- and non-coronary leaflets ($\alpha = 135^{o}$).

The three different inlet widths used were based on the assumption that the bicuspid aortic valve pathology progresses towards stenosis, with the width of the inlet decreasing gradually over time. Figure 2.4 illustrates the inlet to the aorta, showing the relationship between the radius of the aorta, *R*, and the radius of the inlet, *r*. The idea of using an ellipse to represent the inlet area came from prior work done by Viscardi et al., who found the elliptical inlet to provide valid information about the realistic geometry [34]. The radius of the aorta was kept constant at 1.5 cm and the radius of the inlet was investigated at values equal to 70% R, 50% R, and 30% R.

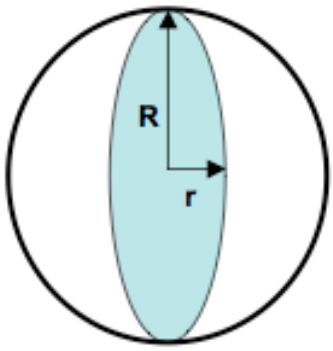

Figure 2.4 Inlet to the aorta

2.3 The Mathematical Model

In order to analyze the blood flow mechanics, the Navier-Stokes equations for incompressible fluids are used as follows. If we take t=0 as the initial time of the analysis, then the following system of partial differential equations must be solved for $t > 0$:

$$\rho\frac{\partial \boldsymbol{u}}{\partial \mathrm{t}} + \rho(\boldsymbol{u} \bullet \nabla)\boldsymbol{u} + \nabla \mathrm{P} - \mathrm{div}(2\mu \boldsymbol{D}(\boldsymbol{u})) = \boldsymbol{f}$$

$$\mathrm{div}\,\boldsymbol{u} = 0 \qquad \text{(E. 1)}$$

where the spatial domain $\Omega \subset \boldsymbol{R}^3$ represents the interior of the vessel under investigation [3]. The first equation represents the conservation of linear momentum, and is formed by three scalar differential equations, one for each component of the velocity. The second is the continuity equation, and represents the conservation of mass. As previously said, the domain $\boldsymbol{\Omega}$ is fixed with time. In non-Newtonian models the viscosity μ is a function of the *strain rate,*

$$\boldsymbol{D}(\boldsymbol{u}) = \frac{\nabla \boldsymbol{u} + \nabla \boldsymbol{u}^T}{2}, \qquad \text{(E. 2)}$$

but since we are considering Newtonian behavior in this model, μ is kept constant at 0.035 poise. The unknowns are the velocity $\boldsymbol{u}$ and the pressure P. The term $\boldsymbol{f}$ accounts for the possible effects of all external body forces, such as gravity, but is often taken to be zero in hemodynamics, and the constant ρ is fluid density, which is equal to 1 g/ml in this model [3].

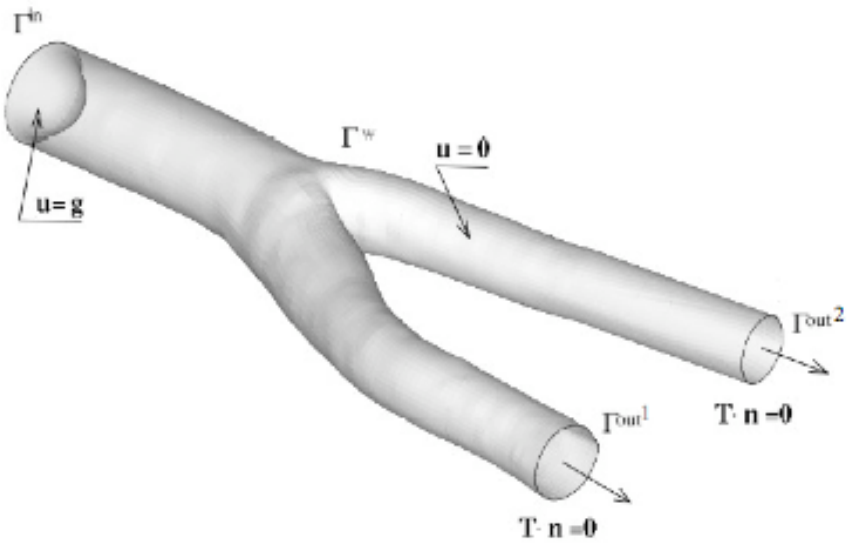

Figure 2.5 Model of a carotid bifurcation, illustrating a typical computational domain [3].

In addition to these equations, boundary conditions on $\partial\Omega = \Gamma^{wall} \cup \Gamma^{in} \cup \Gamma^{out1} \cup \Gamma^{out2}$ have to be prescribed (figure 2.5). The inflow (Γ^{in}) and outflow ($\Gamma^{out1}, \Gamma^{out2}$) boundaries are often described as *artificial boundaries*, as they do not correspond to a physical interface, but are used to separate the region of interest. To reproduce a given blood flow rate typically a velocity profile is prescribed at the "inflow" boundary (Dirichlet boundary conditions). This was done in this project with Γ^{in} being in this case a circular section representing the inlet to the aorta. A zero velocity was prescribed at the walls of the aorta corresponding to a *no-slip* condition for blood particles in contact with the (rigid) wall. Finally, the *normal stresses* at the distal (or outflow) boundaries of the aorta was also prescribed as zero (Neumann boundary conditions) [3]. Normal stress is defined as $\mathbf{T}\cdot\mathbf{n}$, where $\boldsymbol{n}$ is the normal vector to the considered boundary section and $\boldsymbol{T}$ is the *Cauchy stress tensor*,

$$\boldsymbol{T} = -\mathrm{P}\,\boldsymbol{I} + 2\mu\boldsymbol{D}(\boldsymbol{u}) \qquad \text{(E. 3)}$$

P being the pressure, ***I*** the identity matrix, μ the viscosity of the fluid and ***D(u)*** the *strain rate* as defined in E.2 [3]. In the simulations hereby discussed, the velocity profile prescribed at the inflow boundary was defined as an elliptical paraboloid, whose axis of symmetry is normal to the inlet section. Considering a Cartesian coordinate system, whose origin is the center of the circular inlet section, the inflow velocity vectors are directed along the *z*-axis, that is along the inward normal to Γ^{in}, and the velocity magnitude $\bar{\boldsymbol{u}}$ is expressed as,

$$\bar{\boldsymbol{u}}(\boldsymbol{x},\boldsymbol{y},\boldsymbol{t}) = \boldsymbol{Q}(\boldsymbol{t})\frac{2}{\pi \mathrm{rR}}\left(1 - \frac{\boldsymbol{x}^2}{\mathrm{R}^2} - \frac{\boldsymbol{y}^2}{\mathrm{r}^2}\right) \qquad \text{(E. 4)}$$

where *t* is the time, *x* and *y* are the Cartesian coordinates in the plane containing Γ^{in}, *R*=1.5 cm is the radius of the aorta, *r* is half the width *w* of the effective inlet (see figure 2.1), which is varied, and *Q(t)* is the time-varying *flow rate,* as can be seen in figure 2.6. The flow rate is given by (see figure 2.7),

$$\boldsymbol{Q}(\boldsymbol{t}) = \tilde{\boldsymbol{Q}}\sin\frac{\pi \mathrm{t}}{\tau} \quad \text{if } \mathrm{t} < \tau \text{ and } \boldsymbol{Q}(\boldsymbol{t}) = 0 \text{ otherwise}, \qquad \text{(E. 5)}$$

where $\tilde{\boldsymbol{Q}}$ = 485 ml/s is the peak flow rate and τ=0.3 s is the duration of systole, (i.e. left ventricle contraction) [35]. The numerical simulations performed in the present work refer to the systolic phase, when most of the significant phenomena under examination are expected to occur. In fact, in the described numerical setup, the solution dynamics are expected to be strongly dominated by the boundary conditions and to have a relatively small dependence on the initial condition.

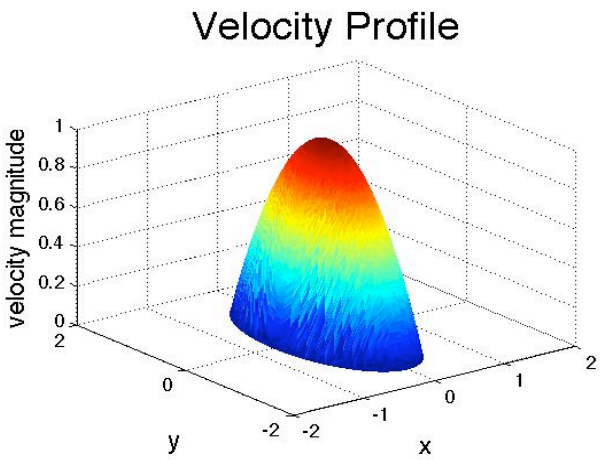

Figure 2.6 Parabolic velocity profile prescribed at the inlet section of the computational domain (with r = 0.75 cm). The amplitude has been normalized to 1.

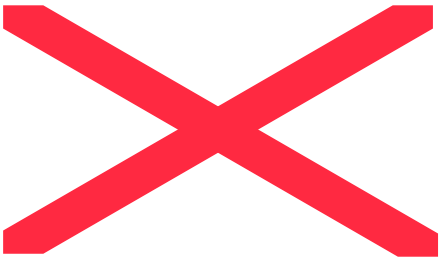

Figure 2.7 The time-varying flow rate as defined by equation (5).

2.4 Quantitative Analysis

The goal is to identify a quantitative correlation between the blood flow features induced by the shape of the bicuspid aortic valve and the location of aortic regions where pathologies, such as aortic dilation, develop. In addition to images (when available) and blood flow velocity measurements, numerical methods for the computation of significant fluid dynamic indexes, such as wall

shear stress, have to be considered in order to complete the overall picture provided by the data.

One hemodynamic variable that will be considered is pressure, as it could be an important indicator for the pathology [36]. Pressure and velocity are directly computed by solving the Navier-Stokes equations. It is possible to compute other important hemodynamic variables that might be other indicators for aortic dilation: the *stresses*, and in particular the wall shear stress. Wall shear stress (WSS) is the component of the normal stresses tangential to the wall, that is, the force per unit area that the fluid exerts tangentially on the wall of the vessel. It is defined mathematically as

$$\mathrm{WSS} = \mu(\nabla \boldsymbol{u} + \nabla \boldsymbol{u}^T) \cdot \boldsymbol{n} - (\mu \boldsymbol{n} \cdot (\nabla \boldsymbol{u} + \nabla \boldsymbol{u}^T) \cdot \boldsymbol{n})\boldsymbol{n} \qquad \text{(E. 6)}$$

where $\boldsymbol{n}$ is the unit vector normal to the wall. Wall shear stress induced by blood flow has been associated with the development of atherosclerosis, and in particular low and oscillating values of WSS have been associated with the development of atherosclerotic plaques in the carotid arteries [37, 38]. In the aortic arch, development of atherosclerotic regions has been observed to occur particularly in regions of extrema (minima and maxima) in wall shear stress and pressure [36]. Therefore it is viable to assume that wall shear stress could be strongly correlated with the development of pathologies in the aortic arch.

2.5 Numerical Approximation

In order to carry out the simulations, modeling and numerical computations explained earlier, scientific computing software titled LifeV was used. The

development of LifeV started in 1999 as a joint collaboration of three institutions: Ecole Polytechnique Federale de Lausanne (CMCS) in Switzerland, Politecnico di Milano (MOX) in Italy and Institut National de Recherche en Informatique et en Automatique (REO) in France. Since 2008 Emory University's Department of Mathematics and Computer Science has become a part of the development team. LifeV is a finite element software library implemented in C++ language collecting algorithms for solving systems of 2-D and 3-D partial differential equations that arise from mathematical modeling of physical problems, such as fluid dynamics, fluid-structure interactions, flow in porous media, and electrocardiology. LifeV contains a core part that provides data structures for the implementation of *Galerkin finite element methods* for solving partial differential equations, as well as a set of solvers for specific applications, such as the Navier-Stokes solver. The LifeV library is organized into layers, the most external of which is called `testsuite`. This layer collects the implementations of specific applications or simple tests to check the proper functioning of the library. *Testsuite* requires user-defined data that specifies the features of the desired test. It is this layer of LifeV that was modified in the simulations and modeling involved in this project. LifeV is capable of importing different mesh formats, such as the ones generated by Gambit[1], Netgen[2] and Cubit[3] and it relies on visualization software such as Paraview[4] and Ensight[5], concerning data processing.

[1] http://www.anys.com/
[2] http://sourceforge.net/projects/netgen-mesher/
[3] http://cubit.sandia.gov/
[4] http://www.paraview.org/
[5] http://www.ensight.com/

2.6 Summary

This project used CFD to investigate a small region of the aorta, starting at the junction with the left ventricle. A fine mesh of a simplified, or "candy cane," aortic geometry with about 14,000 vertices and 67,000 volumes was created using Netgen (figure 2.8). The geometry assumes rigid walls and represents the hemodynamics during the systolic phase. There were a total of nine numerical simulations run on this geometry in order to account for a wide range of inlet size and angle combinations. One additional simulation was performed on a realistic aortic geometry, to compare the results obtained in an idealized situation with the findings of a patient specific blood flow simulation. The corresponding mesh was also created using Netgen and had a similar number of vertices and volumes (Figure 2.8). It had an inlet angle of about 90^{o} and an inlet radius of about 40%R (0.42 cm). The finite element code LifeV was used to perform these simulations. Blood was assumed to be a Newtonian fluid, homogenous and incompressible, so that the Navier-Stokes equations for incompressible fluids could be used for the mathematical description. Wall shear stress was computed after obtaining the pressure and velocity fields from the Navier-Stokes equations, and all three hemodynamic variables were analyzed using the visualization software Paraview.

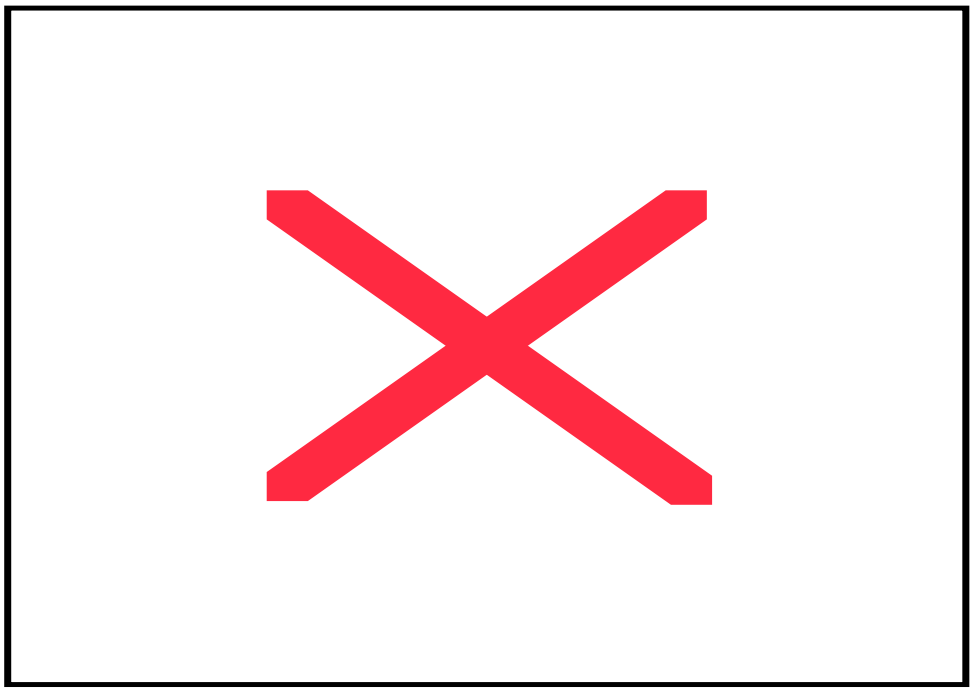

Figure 2.8 Images of meshes. *(a)* The idealized geometry, *(b)* The realistic geometry.

3. Results

The numerical results for velocity, pressure and wall shear stress of blood in the reconstructed aortic geometries obtained from LifeV were analyzed using the Paraview visualization software. There were a total of nine simulations performed on the idealized geometry, one for each combination of inlet width and angle. Recall that the three inlet angles considered were 90^{o} (fusion of the right- and left-coronary cusps), 45^{o} (fusion of the left- and non-coronary cusps), and 135^{o} (fusion of the right- and non-coronary cusps) and that the three inlet widths observed were 30%R (0.45 cm), 50%R (0.75 cm), and 70%R (1.05 cm). The vectors of the velocity field at peak systole (0.15 s) can be seen below in figure 3.1 for all nine simulations in the idealized geometry. Each row shows a different inlet width and each column shows a different inlet angle. The velocity range is the same for

each inlet angle, but differs for each inlet width. The maximum velocity for an inlet width of 30%R is 432 cm/s, which is significantly larger than that of 70%R which is 193 cm/s, or 50%R which is 271 cm/s, making it difficult to display velocity values on the same scale.

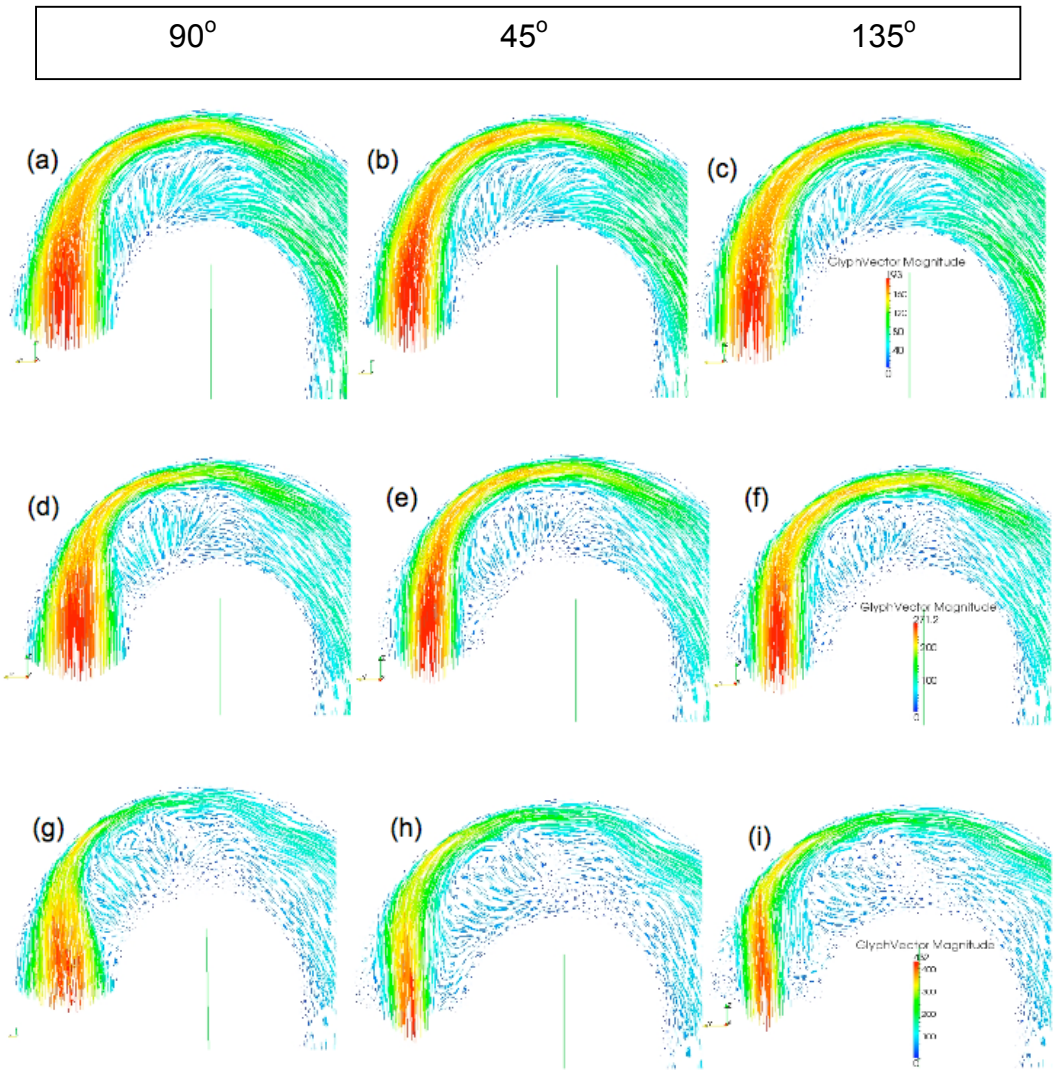

Figure 3.1 Velocity profile at peak systole (time=0.15 s). Arrows represent velocity vectors in the symmetry plane of the geometry. Arrows length is proportional to the velocity magnitude.
(a) Inlet with radius r = 1.05cm and angle $\alpha = 90^{o}$, *(b)* Inlet with r = 1.05cm and angle $\alpha = 45^{o}$, *(c)* Inlet with r = 1.05cm and angle $\alpha = 135^{o}$, *(d)* Inlet with r = 0.75cm and angle $\alpha = 90^{o}$, *(e)* Inlet with r = 0.75cm and angle $\alpha = 45^{o}$, *(f)* Inlet with r = 0.75cm and angle $\alpha = 135^{o}$, *(g)* Inlet with r = 0.45cm and angle $\alpha = 90^{o}$, *(h)* Inlet with r = 0.45cm and angle $\alpha = 45^{o}$, *(i)* Inlet with r = 0.45cm and angle $\alpha = 135^{o}$

Figure 3.3 shows a cross-view of the velocity magnitude (*speed*) pattern at the top of the aortic arch (figure 3.2) during peak systole for all nine simulations on the idealized geometry. The images are arranged in the same manner as 3.1, with the same inlet width in each row and inlet angle in each column. This view highlights both the asymmetry caused by flowing through a bend in the geometry and the asymmetry induced by rotating the inlet angle. It can be seen that the asymmetry from the rotation of the inlet angle becomes more pronounced as the width of the inlet is decreased. The velocity profiles for an inlet radius of 1.05 cm almost appear symmetric, despite the rotation of the inlet.

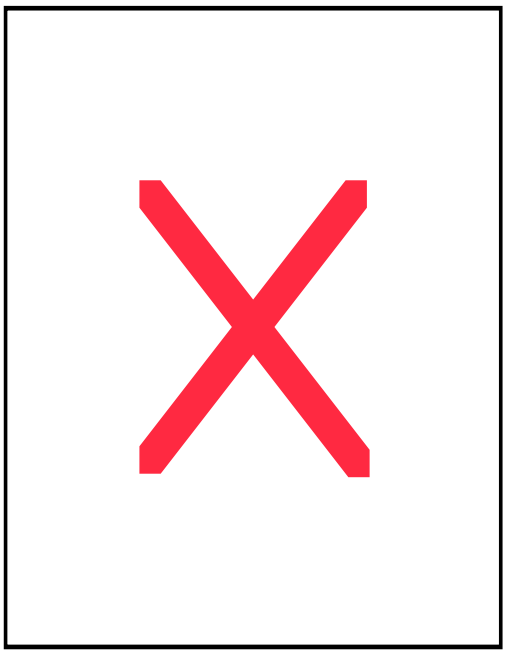

Figure 3.2 Location of cross-sectional velocity slice.

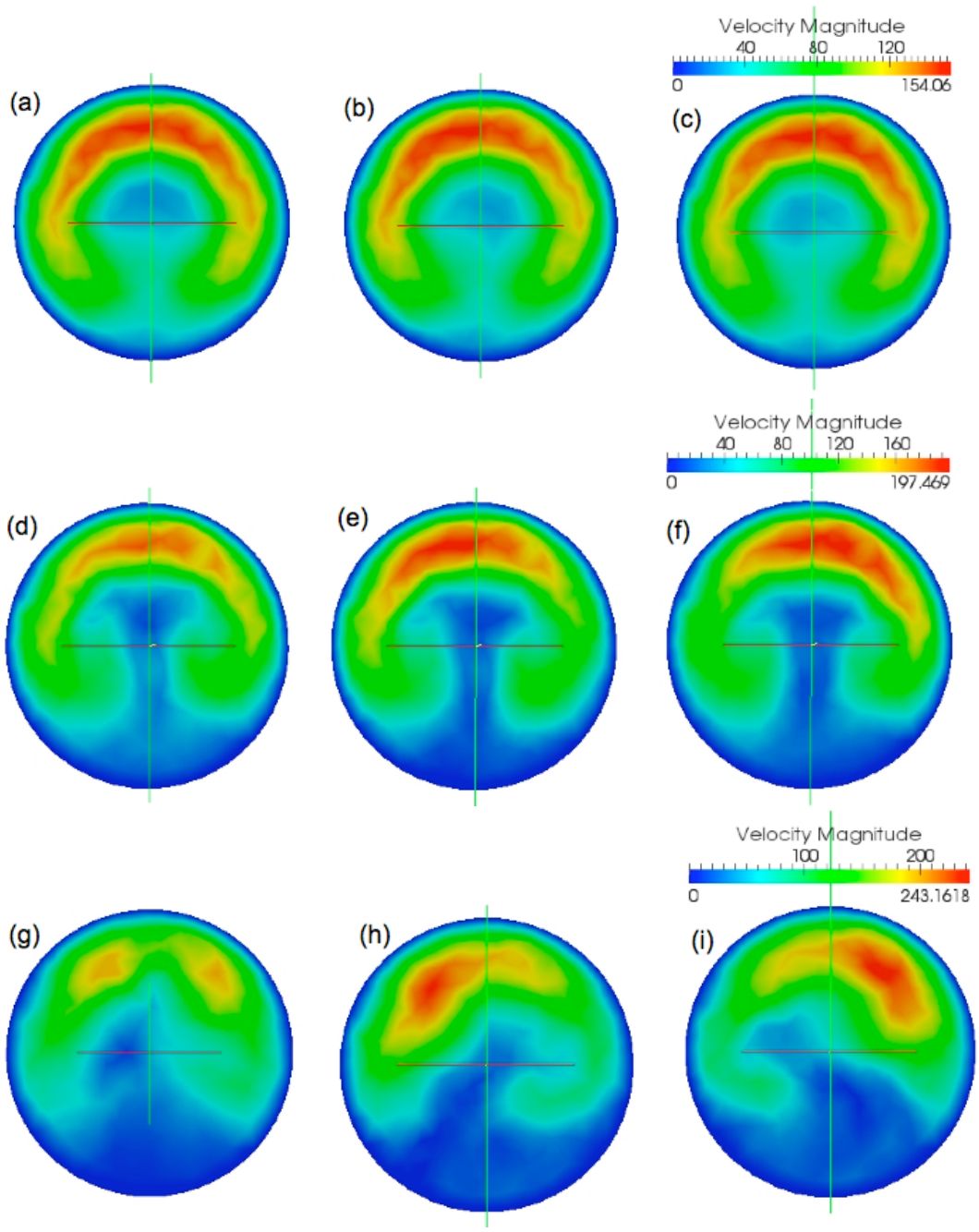

Figure 3.3 Velocity magnitude cross-section profile at top of aortic arch during peak systole.
(a) Inlet with radius $r = 1.05$cm and angle $\alpha = 90^{o}$, *(b)* Inlet with $r = 1.05$cm and angle $\alpha = 45^{o}$, *(c)* Inlet with $r = 1.05$cm and angle $\alpha = 135^{o}$, *(d)* Inlet with $r = 0.75$cm and angle $\alpha = 90^{o}$, *(e)* Inlet with $r = 0.75$cm and angle $\alpha = 45^{o}$, *(f)* Inlet with $r = 0.75$cm and angle $\alpha = 135^{o}$, *(g)* Inlet with $r = 0.45$cm and angle $\alpha = 90^{o}$, *(h)* Inlet with $r = 0.45$cm and angle $\alpha = 45^{o}$, *(i)* Inlet with $r = 0.45$cm and angle $\alpha = 135^{o}$

The pressure patterns during peak systole for all nine simulations were also observed, as can be seen below in figure 3.4. The images are arranged in the same manner as the previous figures.

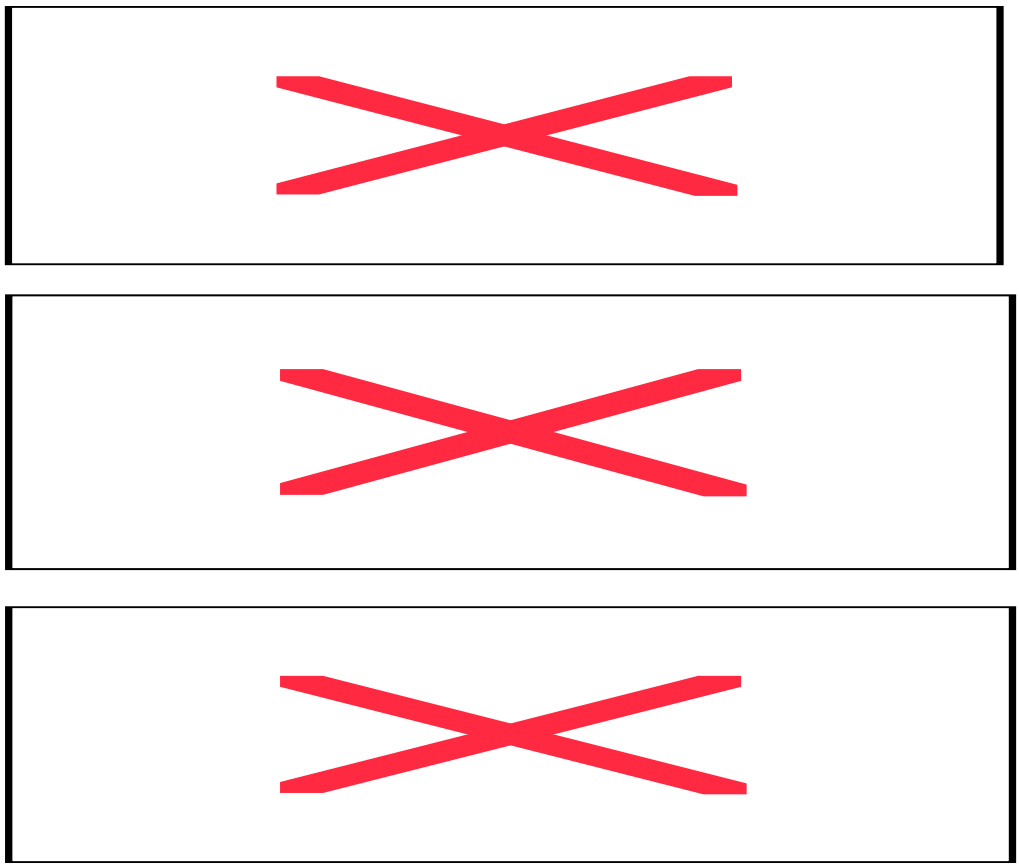

Figure 3.4 Pressure pattern during peak systole in the symmetry plane of the geometry. *(a)* Inlet with radius r = 1.05cm and angle $\alpha = 90^{o}$, *(b)* Inlet with r = 1.05cm and angle $\alpha = 45^{o}$, *(c)* Inlet with r = 1.05cm and angle $\alpha = 135^{o}$, *(d)* Inlet with r = 0.75cm and angle $\alpha = 90^{o}$, *(e)* Inlet with r = 0.75cm and angle $\alpha = 45^{o}$, *(f)* Inlet with r = 0.75cm and angle $\alpha = 135^{o}$, *(g)* Inlet with r = 0.45cm and angle $\alpha = 90^{o}$, *(h)* Inlet with r = 0.45cm and angle $\alpha = 45^{o}$, *(i)* Inlet with r = 0.45cm and angle $\alpha = 135^{o}$

The maximum pressure is 35,628 in the simulations with an inlet radius of 0.45 cm, which is approximately three-fold higher than the maximum velocity of 9,387 in the simulations with an inlet radius of 1.05 cm. The region where the maximum pressure is located appears approximately the same in all nine

simulations, despite the differences in inlet width and angle. However, it appears as though the size of the region of high pressure may be slightly smaller in the geometry with the smallest inlet width, which is most likely due to the more concentrated inflow jet.

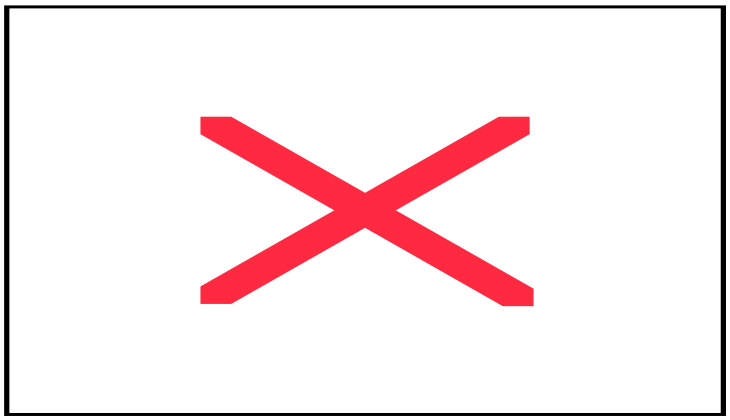

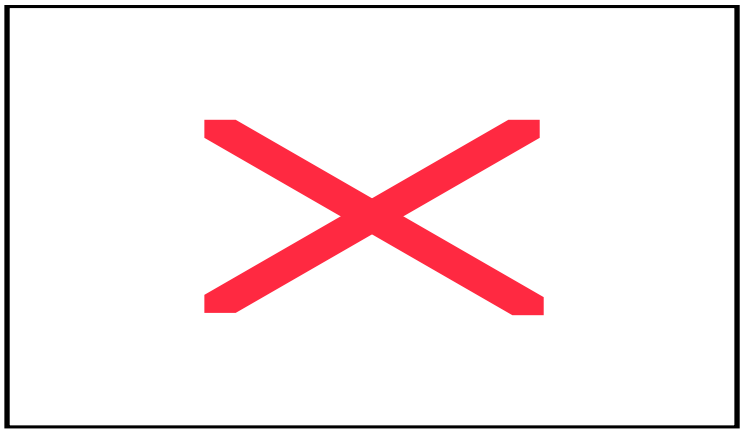

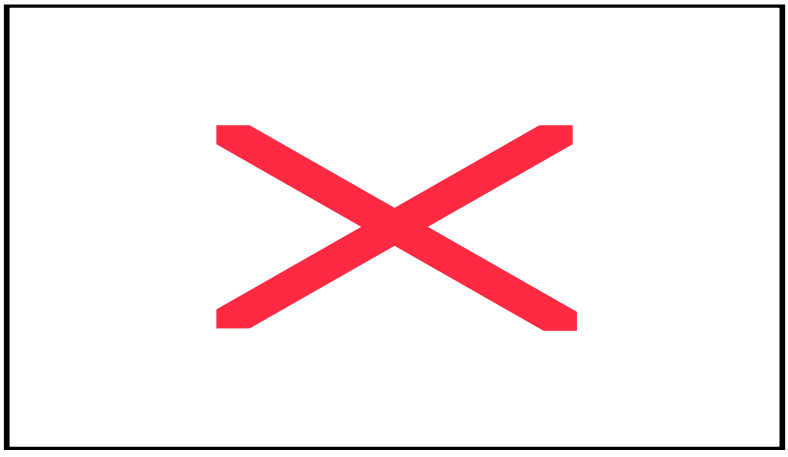

Figure 3.5 Wall shear stress (WSS) magnitude pattern during peak systole. The view is of the top of the aortic arch, looking down, with the inlet located at the top of the image. *(a)* Inlet with radius $r = 1.05$cm and angle $\alpha = 90^o$, *(b)* Inlet with $r = 1.05$cm and angle $\alpha = 45^o$, *(c)* Inlet with $r = 1.05$cm and angle $\alpha = 135^o$, *(d)* Inlet with $r = 0.75$cm and angle $\alpha = 90^o$, *(e)* Inlet with $r = 0.75$cm and angle $\alpha = 45^o$, *(f)* Inlet with $r = 0.75$cm and angle $\alpha = 135^o$, *(g)* Inlet with $r = 0.45$cm and angle $\alpha = 90^o$, *(h)* Inlet with $r = 0.45$cm and angle $\alpha = 45^o$, *(i)* Inlet with $r = 0.45$cm and angle $\alpha = 135^o$

Figure 3.5 (above) shows the wall shear stress magnitude pattern of the blood against the aortic wall during peak systole. The images are arranged in the same fashion as the previous figures. The view is of the top of the aortic arch, looking down, with the inlet located at the top of the image. As seen with pressure, the area of highest wall shear stress is located in approximately the same position for all nine simulations, however, the magnitude and surface area of the high wall shear stress region increases as the inlet size decreases. The maximum value for wall shear stress is 35.3 dyn/cm^2 when the inlet radius is 1.05 cm and is almost doubled at a maximum of 54.8 dyn/cm^2 when the inlet radius is 0.45 cm. When looking at the medium wall shear stress areas (green), it appears as though this region is located more proximal (closer) to the inlet in the geometries with smaller inlets. It is also possible to see the asymmetry induced by the inlet angle, especially when $r = 0.75$ cm or 0.45 cm. The images of inlet angles of 45^o and 135^o look like mirror images of each other, which was somewhat expected by symmetry considerations.

The following figures (3.7 and 3.8) show the velocity magnitude (speed) isolines in four of the nine different simulations during peak systole (0.15 s). The isolines for three different cross-sectional slices from each geometry were computed in order to investigate in more detail the effects of an 180^o bend in the

geometry and what role the inlet size and angle play. One slice was taken at the top of the aortic arch, as in figure 3.3, and two slices were taken more distal from the inlet, as can be seen in figure 3.6. One of these slices was taken at the same height as the inlet and the other was taken 5 cm below the inlet height.

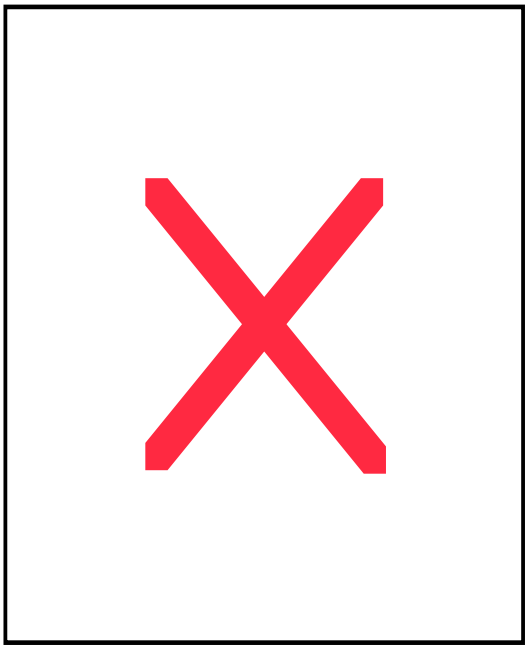

Figure 3.6 Location of three different cross-sectional slices for which the speed isolines were computed. Slice 1 is at the top of the aortic arch, slice 2 is at the same height as the inlet, and slice 3 is 5 cm below the height of the inlet.

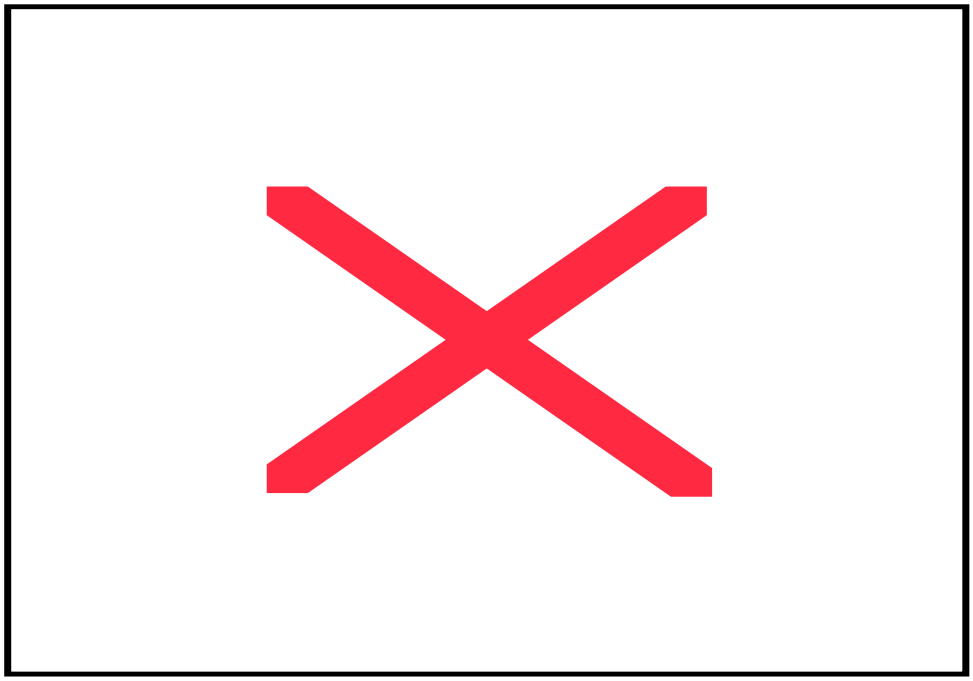

Figure 3.7 Speed isolines for an inlet radius of 70%R (1.05 cm) at peak systole. The view is in the direction of blood flow, and the numbers correspond to figure 3.6. *(a)* Inlet angle of 90°, *(b)* Inlet angle of 45°. The color scales are the same in both (a) and (b).

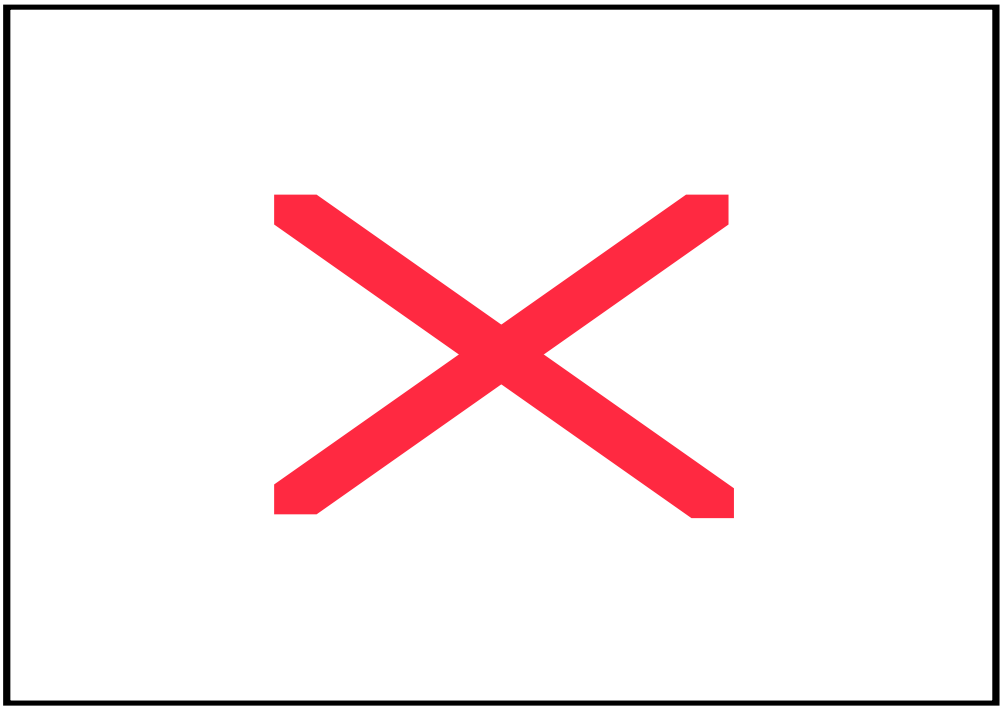

Figure 3.8 Speed isolines for an inlet radius of 30%R (0.45 cm) at peak systole. The view is in the direction of blood flow, and the numbers correspond to figure 3.6. *(a)* Inlet angle of 90°, *(b)* Inlet angle of 45°. The color scales are the same in both (a) and (b).

Only the largest and smallest inlet widths were investigated because it can be assumed that the medium-sized inlet width would have intermediate results, and looking at the two extremes provides a more interesting analysis. It has also been seen that the results for 45° and 135° tend to be mirror images of each other, and so the results for 135° were omitted. In figure 3.7 it can be seen that *(a)* and *(b)*

look the same despite the inlet rotation. In figure 3.8 it appears that the inlet angle only alters the symmetry of slice 1 and that the other two slices look the same despite the different inlet angle. More precisely, slice 3 looks the same for both inlet widths, and slice 2 looks similar. Slice 1 is the most altered due to inlet size and angle.

As the blood flows around the 180^{o} bend of the aortic arch the rings become distorted by gradients in velocity and no longer form symmetric, concentric circles as would be seen if the geometry were straight. Slice 3 shows the blood returning to this conformation. When the inlet radius is 1.05 cm the isolines in slice 1 show a sort of "banana" shape along the top (figure 3.7, 1(a)), as would be expected if the inlet were completely open [39]. It is interesting to observe that when the inlet radius in only 0.45 cm, it looks as though the "banana" was squeezed in the middle (figure 3.8, 1(a)). Figure 3.8, 1(b) shows that the "banana" profile has disappeared completely when the smaller inlet has been rotated 45^{o}, which could possibly have some interesting effects. In all four simulations, it can be seen that in slice 1, the lines are closest at the top of the slice, indicating a higher gradient (i.e. faster change in velocity) in proximity to the wall.

One numerical simulation was performed on a realistic aortic geometry and the velocity, pressure and wall shear stress were computed. Figure 3.10 shows both the side view of the velocity vector field and the velocity pattern of a cross-sectional slice at the top of the arch during peak systole, and figure 3.9 shows the exact location of these slices. The maximum velocity is about 196 cm/s, which is

almost exactly the same value as the maximum velocity of the idealized geometry with the large inlet, which was 193 cm/s. The velocity pattern at the top of the aortic arch illustrates the "banana" shape much like the results of the large inlet on the idealized simulations. However, it is asymmetric, which must be due to the geometry difference in shape of the arch. It resembles the velocity pattern of the smallest inlet width with an angle of 45^{o} in that it has the region of highest velocity only on one side of the "banana" shape.

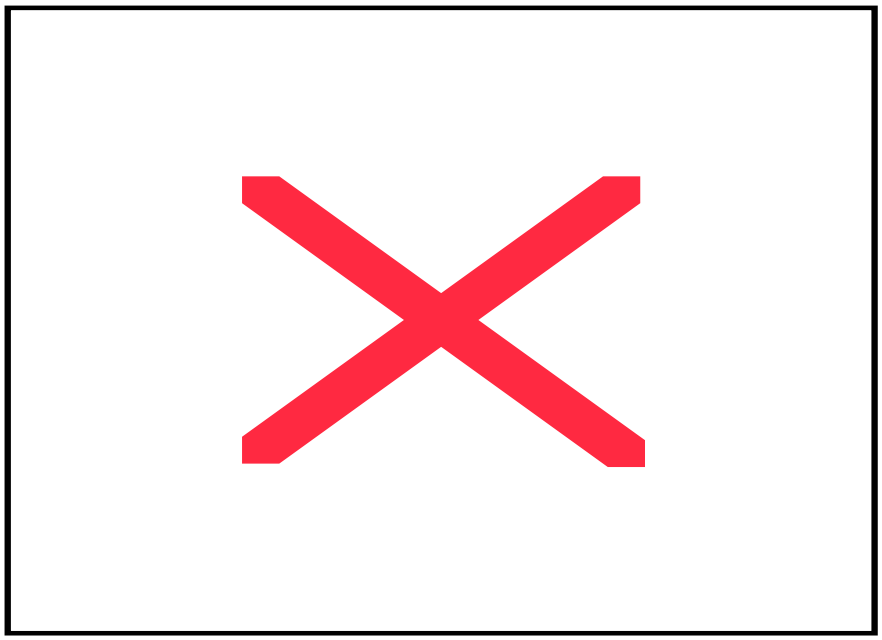

Figure 3.9 Location of slices of velocity and pressure patterns in realistic geometry

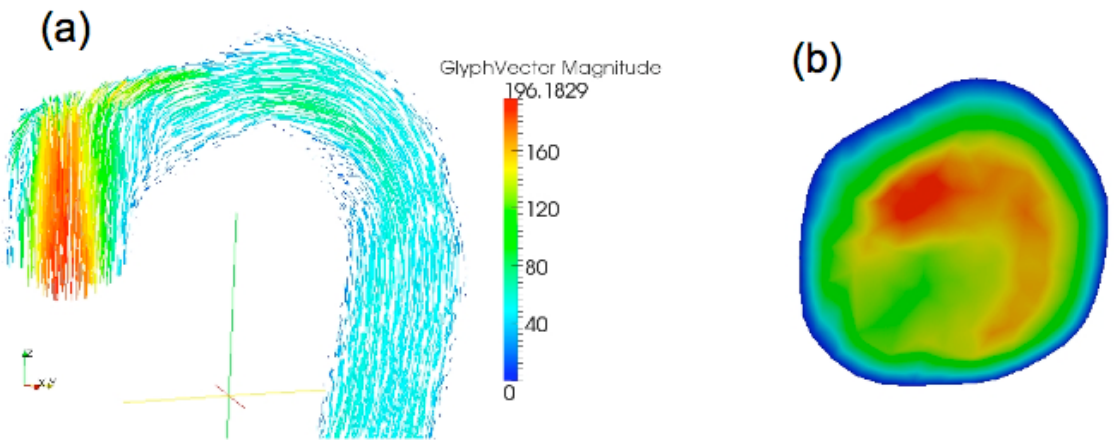

Figure 3.10 Velocity patterns in realistic aortic geometry at peak systole. *(a)* Side view of velocity vector field, *(b)* Cross-sectional view of velocity pattern at top of aortic arch.

The pressure pattern was also observed during peak systole and can be seen below in figure 3.11. It appears to be quite similar to all of the simulations performed on the idealized geometries in that there is a region of high pressure along the top of the aorta where the concentrated blood flow jet hits the wall of the aorta. The maximum pressure value is 18,226, which is very similar to the maximum pressure value of the simulations where the inlet radius was 0.75 cm (the intermediate inlet width), which is 17,123.

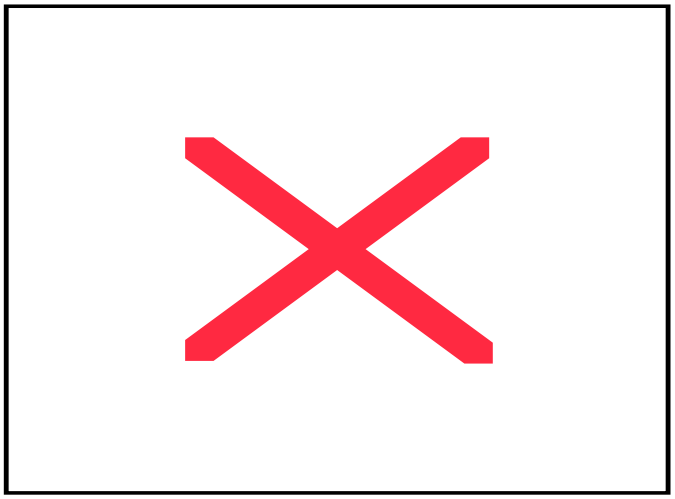

Figure 3.11 Pressure pattern in realistic aortic geometry at peak systole.

Finally, the wall shear stress was observed in the realistic geometry, as seen in figure 2.12. It is similar to the results for the idealized geometry in that there is a region of high wall shear stress at the top of the arch, but there is an additional region of high wall shear stress more proximal to the inlet. This is most similar to the wall shear stress pattern of the simulations with an inlet radius of 0.45 cm (the smallest inlet), because they showed higher levels of wall shear stress near the inlet then the other radii. The maximum value of wall shear stress in the realistic case is about 26 dyn/cm^2, which is closest to the maximum value for the simulations with the largest inlet radius (1.05 cm), which was about 35 dyn/cm^2.

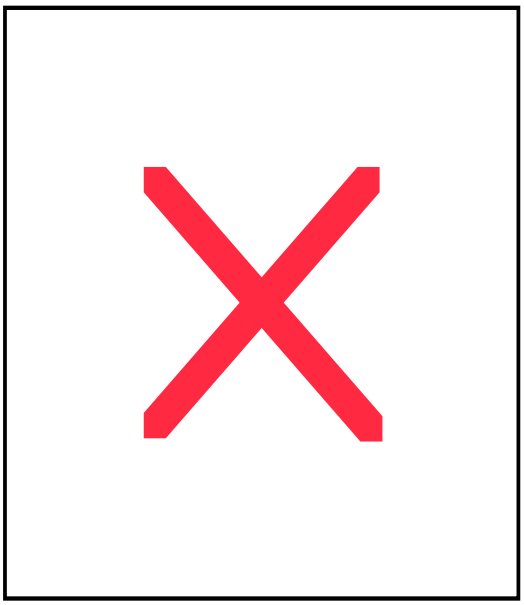

Figure 3.12 Wall shear stress in realistic aortic geometry at peak systole. The view is of the top of the aortic arch, looking down, with the inlet located at the top of the image.

4. Discussion

Computational fluid dynamic modeling has been widely used to predict pathologies in the cardiovascular system, even in the aortic arch [36]. However, the use of CFD models with finite element analysis to understand the hemodynamic mechanisms that contribute to aortic dilation in patients with bicuspid aortic valves is an unconventional approach, as there is little or no prior work on this in the literature. Some preliminary results can be found in the work of F. Viscardi et al. [34]. Due to the lack of prior studies and the limit of the present work, we made several assumptions to define the model. As mentioned earlier, these assumptions included the rigid, "candy cane" shaped geometry, the non-moving, open valve, treating blood as a Newtonian fluid, and the shape and size of the inlet. The geometry did not account for the vessels coming out of the aorta, because there was not enough data to usefully reconstruct these vessels, and there was also not enough data available to generate patient specific geometries and boundary conditions. However, the purpose of this project was to look at the main features of blood flow in the aorta with a bicuspid aortic valve, which this simplified geometry still provides, and moreover, to test CFD as a suitable tool for investigating this kind of problem. It must be pointed out that certain quantities, such as wall shear stress, are difficult to obtain in patients, and so there were not measurements to compare with the results. Because of these assumptions and limitations, the data generated by these idealized simulations is only qualitatively relevant at this time.

The results show that as the size of the inlet decreases, the velocity, pressure and wall shear stress all increase in the ascending aorta. The large inlet simulations with an inlet radius of 1.05 cm show no asymmetry induced by rotation of the inlet and have significantly lower values for velocity, pressure and wall shear stress than the other two inlet width values, and so it may be assumed to be equivalent to the tricuspid (healthy) aortic valve case. Additionally, the area of the region of maximum pressure decreases and the location of the moderate levels of wall shear stress are more proximal to the inlet with the decreasing inlet radius. As mentioned earlier, areas of extrema in wall shear stress and pressure have been correlated with the formation of atherosclerotic regions, it is therefore reasonable to consider the possibility that these high-pressure and high-wall shear stress regions induced by narrow inlets may be correlated with the development of atherosclerotic plaques [36]. Additionally, blood vessel wall remodeling is associated with prolonged increases of pressure and flow rate, and so narrow inlets may be correlated with aortic dilation.

It is unclear how the inlet angle is correlated with pathologies of the aortic arch. It can be seen that for the two smaller inlet radii (0.75 cm and 0.45 cm), the rotation of the inlet angle induces asymmetry of the blood flow, but it is difficult to predict the effect of the asymmetry. Prior studies have suggested that pathologies, such as aortic stenosis and aortic dilation, are more common in patients with fusion of the right-coronary and non-coronary leaflets (135^{o}), however these findings did not reach statistical significance [14, 18, 19]. It would make sense that the inlet angle of 45^{o} would result in a similar number of aortic

pathologies since the blood flow dynamics are the mirror image of the 135^{o} case, but fusion of the left-coronary and non-coronary leaflets only occurs in about 2% of BAV patients compared with the 26% of patients with the right-coronary and non-coronary leaflets fused. This could at least partially account for the discrepancy. It is also worth noting that the increased asymmetry is correlated with decreased inlet widths, and so it is possible that pathologies are correlated with the effects of both inlet width and angle simultaneously. It would be especially interesting to research whether fusion of the right-coronary and non-coronary leaflets is correlated with a smaller inlet area than the other BAV morphologies.

The run on the realistic geometry appears to be a sort of hybrid of the results of the idealized geometries. The observed maximum values of the velocity and wall shear stress were most like those of the simulations run on geometries with an inlet width of 1.05 cm, and the maximum value for pressure was similar to that of an inlet radius of 0.75 cm. However, the patterns of the velocity, pressure and wall shear stress appeared more like those of an inlet radius of 0.75 cm or 0.45 cm. The asymmetry is most likely explained by the asymmetric geometry inherent in the human aorta, but it remains unclear why the maximum values were lower, since the inlet radius was only about 0.42 cm (about 40% of the aorta radius at the inlet). The similarity in values and patterns to the idealized geometries suggests that the model is valid, although more research needs to be done in order to investigate why the realistic geometry seems to have qualities of all three of the inlet radii instead of being clearly assimilated to just one.

5. Conclusion

Comparison of the nine simulations for the different bicuspid aortic valve models shows an increase in flow velocity, pressure and wall shear stress correlated with a decrease in the width of the effective inlet. There is also an asymmetric flow pattern correlated with inlet angles of 45^{o} and 135^{o}, but only in the two smaller inlets. At this point in the research it can be concluded that there is something inherent with blood flow in the aortic arch in models with bicuspid aortic valves that is intrinsically different from the normal tricuspid aortic valve flow. Additionally, this flow differs depending on the specific morphology of the bicuspid aortic valve under investigation.

There are two potential different paths in which the continued research of this project may proceed. The first is that additional inlet conditions be investigated on the idealized geometry. As mentioned earlier in the paper, there are five degrees of freedom for inlet conditions and the simulations carried out in this research project only considered two of them. The other inlet conditions that need to be considered are the vertical offset of the inlet, the horizontal offset of the maximum opening of the inlet section, and the angle of the inflow velocity with respect to the orientation of the inflow section (figure 2.1). The other path in which the research may proceed is to use a patient specific data for the simulations. This data would include parameters characterizing the blood and vessel walls (such as wall mass density) and geometrical data so that the computational domain could be accurately defined. The vessel walls would no longer be rigid and the movement of the valve may want to be considered. This

path would be much more difficult to follow, as it is difficult to obtain such detailed patient specific data.

6. Glossary

Aortic Aneurysm – a condition in which there is a bulge in a section of the aorta due to a weak artery wall. The aneurysm may burst, which can cause serious bleeding that can quickly lead to death [40].

Aortic Dilation – a condition in which the aortic root is enlarged. This may pull the leaflets of the valve apart and out of shape, causing them to leak (regurgitation) [1].

Aortic Dissection – a condition in which a tear develops in the inner layer of the aorta. This allows blood to pass into the middle layer of the aorta, causing the inner and middle layers to separate. The blood-filled section may rupture through the outer aortic wall, which often results in death [41].

Aortic Regurgitation – a condition where the aortic valve does not close tightly, which allows some blood to leak backwards through the valve and back into the left ventricle. If the leak is bad enough, the heart must work harder to make up for the defective valve, and less blood may flow to the rest of the body [1].

Aortic Stenosis – a condition where the aortic valve opening is smaller than normal due to stiff or fused leaflets. This may cause the heart to work very

hard to pump blood through it, which may lead to heart failure or other symptoms [42].

Infective Endocarditis – a bacterial infection of the inner lining of the heart muscle. If left untreated, multiplying bacteria may eventually destroy the heart valves and result in heart failure. The bacteria may also form small clots that can move through the blood stream and block small arteries [43].

7. Bibliography

1. Healthwise. Heart disease help center: Aortic valve regurgitation. WebMD, http://www.webmd.com/heart-disease/tc/aortic-valve-regurgitation-overview (accessed March 8, 2010)

2. Robert Bryg. Heart disease guide: How the heart works. WebMD, http://www.webmd.com/heart-disease/guide/how-heart-works (accessed March 8, 2010)

3. Formaggia, Luca, Alfio Quarteroni, and Alessandro Veneziani, eds. 2009. *Cardiovascular mathematics: Modeling and simulation of the circulatory system.* Vol. 1 of *Modeling, simulation and applications*. Milan: Springer-Verlag. Chaps. 1-3.

4. Hoffman, Julien I. E. and Samuel Kaplan. 2002. The incidence of congenital heart disease. *Journal of the American College of Cardiology* 39: 1890-1900.

5. Pick, Adam. Heart murmur from bicuspid valve with two leaflets. The patients guide to heart valve surgery: A special book for patients and caregivers. http://www.heart-valve-surgery.com/Images/bicuspid-aortic-valve.jpg (accessed March 30, 2010)

6. Nistri, S, M.D. Sorbo, M. Marin, M. Palisi, R. Scognamiglio, and G. Thiene. 1999. Aortic root dilation in young men with normally functioning bicuspid aortic valves. *Heart* 82: 19-22.

7. Ward, C. 2000. Clinical significance of the bicuspid aortic valve. *Heart* 83: 81-85.

8. Larsen, E.W. and W.D. Edwards. 1984. Risk factors for aortic dissection: A necropsy study of 161 cases. *American Journal of Cardiology* 53: 849-855.

9. Borger, M.A., M. Preston, J. Ivanov, P.W. Fedak, P. Davierwala, S. Armstrong, and T.E. David. 2004. Should the ascending aorta be replaced more frequently in patients with bicuspid aortic valve disease? *Journal of Cardiovascular Surgery* 128: 677-683.

10. Matsuyama, K., A. Usui, T. Akita, M. Yoshikawa, M. Murayama, T. Yano, H. Takenaka, W. Katou, M. Toyama, M. Okada, M. Sawaki, and Y. Ueda. 2005. Natural history of a dilated ascending aorta after aortic valve replacement. *Circulation* 69: 392-396.

11. Russo, C.F., S. Mazzetti, A. Garatti, E. Ribera, A. Milazzo, G. Bruschi, M. Lanfranconi, T. Colombo, and E. Vitali. 2002. Aortic complications after bicuspid aortic valve replacement: Long-term results. *The Annals of Thoracic Surgery* 74: S1773-S1776; discussion S1792-S1799.

12. Fedak, P.W., S. Verma, T.E. David, R.L. Leask, R.D. Weisel, and J. Butany. 2002.Clinical and pathophysiological implications of a bicuspid aortic valve. *Circulation* 106: 900-904.

13. Gurvitz, Michelle, Ruey-Kang Chang, Stacey Drant, and Vivekanand Allada. 2004. Frequency of aortic root dilation in children with a bicuspid aortic valve. *American Journal of Cardiology* 94:1337-1340.

14. Holmes, Kathryn W., Christoph U. Lehmann, Darshan Dalal, Khuram Nasir, Harry C. Dietz, William J. Ravekes, W. Reid Thompson, and Phillip J. Spevak. 2007. Progressive dilation of the ascending aorta in children with isolated bicuspid aortic valve. *American Journal of Cardiology* 99: 978-983.

15. Cotrufo, M., A. Della Corte, L. S. De Santo, C. Quarto, M. De Feo, G. Romano, C. Amarelli, M. Scardone, F. Di Medlio, G. Guerra, M. Scarano, S. Vitale, C. Castaldo, and S. Montagnani. 2005. Different patterns of extracellular matrix protein expression in the convexity and concavity of the dilated aorta with bicuspid aortic valve: Preliminary results. *Journal of Thoracic Cardiovascular Surgery* 130: 504-511.

16. Fedak, Paul W. M., Mauro P. L. de Sa, Subodh Verma, Nafiseh Nili, Pedram Kazemian, Jagdish Butany, Bradley H. Strauss, Richard D. Weisel, and Tirone E. David. 2003. Vascular matrix remodeling in patients with bicuspid aortic valve malformations: Implications for aortic dilation. *Journal of Thoracic and Cardiovascular Surgery* 126: 797-806.

17. Robicsek, F., M. J. Thubrikar, J. W. Cook, and B. Fowler. 2004. The congenitally bicuspid aortic valve: How does it function? Why does it fail? *Annals of Thoracic Surgery* 77: 177-185.

18. Fernandes, S.M., S. P. Sanders, P. Khairy, K. J. Jenkins, K. Gauvreau, P. Lang, H. Simonds, and S. D. Colan. 2004. Morphology of bicuspid aortic valve in children and adolescents. *Journal of the American College of Cardiology* 44: 1648-1651.

19. Novaro, G. M., I. Y. Tiong, G. I. Pearce, R. A. Grimm, N. Smedira, and B. P. Griffin. 2003. Features and predictors of ascending aortic dilation in association with a congenital bicuspid aortic valve. *American Journal of Cardiology* 92: 99-101.

20. Migliavacca, F., R. Balossino, G. Pennati, G. Dubini, T. Y. Hsia, M. R. de Leval, and E. L. Bove. 2006. Multiscale modeling in biofluidynamics: Application to reconstructive paediatric cardiac surgery. *Journal of Biomechanics* 39: 1010-1020.

21. Quarteroni, Alfio, Alessandro Veneziani, and Paolo Zunino. 2002. Mathematical and numerical modeling of solute dynamics in blood flow and arterial walls. *SIAM Journal on Numerical Analysis* 39: 1488-1511.

22. Hendee, William R., E. Russel Ritenour. 2002. *Medical Imaging Physics.* 4th edition. New York: Wiley-Liss, Inc.

23. Antiga, Luca, Bogdan Ene-Iordache, and Andrea Remuzzi. 2003. Computational geometry for patient-specific reconstruction and meshing of blood vessels from MR and CT angiography. *IEEE Transactions on Medical Imaging* 22(5): 674-684.

24. Cebral, Juan R., Marcelo A. Castro, Sunil Appanaboyina, Christopher M. Putnam, Daniel Millan, and Alejandro F. Frangi. 2005. Efficient pipeline for image-based patient-specific analysis of cerebral aneurysm hemodynamics: Technique and sensitivity. *IEEE Transactions on Medical Imaging* 24(4): 457-467.

25. Bekkers, Erik J. and Charles A. Taylor. 2008. Multiscale vascular surface model generation from medical imaging data using hierarchical features. *IEEE Transactions on Medical Imaging* 27(3): 331-341.

26. Lagana, K., G. Dubini, F. Migliavcca, R. Pietrabissa, G. Pennati, A. Veneziani, and A. Quarteroni. 2002. Multiscale modeling as a tool to prescribe realistic boundary conditions for the study of surgical procedures. *Biorheology* 39(3-4): 359-364.

27. Formaggia, L., J.F. Gerbeau, F. Nobile, and A. Quarteroni. 2001. On the coupling of 3D and 1D Navier-Stokes equations for flow problems in compliant vessels. *Computer Methods in Applied Mechanics and Engineering* 191: 561-482.

28. Blanco, P.J. R.A. Feij´oo and S.A. Urquiza. 2007. A unified variational approach for coupling 3D-1D models and its blood flow applications. *Computer Methods in Applied Mechanics and Engineering* 196(41-44): 4391-4410.

29. Vignon-Clementel, Irene E., C. Alberto Figueroa, Kenneth E. Jansen, and Charles A. Taylor. 2006. Outflow boundary conditions for three-dimensional finite element modeling of blood flow and pressure in arteries. *Computer Methods in Applied Mechanics and Engineering* 195(29-32): 3776-3796.

30. Causin, P., J.F. Gerbeau, and F. Nobile. 2005. Added-mass effect in the design of partitioned algorithms for fluid-structure problems. *Computer Methods in Applied Mechanics and Engineering* 194(42-44): 4506-4527.

31. McQueen, David M. and Charles S. Peskin. Eds. H. Aref and J.W. Phillips. 2001. Heart simulation by an immersed boundary method with formal second-order accuracy and reduced numerical viscosity. In: *Mechanics for a New Millennium, Proceedings of the International Conference on Theoretical and Applied Mechanics (ICTAM) 2000.* Netherlands: Kluwer Academic Publishers.

32. Holzapfel, G.A. and R.W. Ogden. Constitutive modeling of arteries. 2010. Review paper in: *Proceedings of the Royal Society A*.

33. Lerer, P.K. and W.D. Edwards. 1981. Coronary arterial anatomy in bicuspid aortic valve: Necroscopy study of 100 hearts. *Heart* 45: 142-147.

34. Viscardi, F., C. Vergara, L. Antiga, S. Merelli, A. Veneziani, G. Puppini, G. Faggian, A. Mazzucco, G.B. Luciani. Comparative finite-element model analysis of ascending aortic flow in bicuspid and tricuspid aortic valve. To appear in *Journal of Artificial Organs,* 2010.

35. Alastruey, J., K.H. Parker, J. Peiro, S.M. Byrd, and S.J. Sherwin. 2007. Modelling the circle of Willis to assess the effects of anatomical variations and occlusions on cerebral flows. *Journal of Biomechanics* 40(8): 1794-1805.

36. Shahcheraghi, N., H.A. Dwyer, A.Y. Cheer, A.I. Barakat, and T. Rutaganira. 2002. Unsteady and three-dimensional simulation of blood flow in the human aortic arch. *Journal of Biomechanical Engineering* 124(4): 378-388.

37. Zarins, C.K., D.P. Giddens, B.K. Bharadvaj, V.S. Sottiurai, R.F. Mabon, and S. Glagov. 1983. Carotid bifurcation atherosclerosis: Quantitative correlation of plaque localization with flow velocity profiles and wall shear stress. *Circulation Research* 53: 502-514.

38. Friedman, M.H., O.J. Deters, C.B. Bargeron, G.M. Hutchins, and F.F. Mark. 1986. Shear-dependent thickening of the human arterial intima. *Atherosclerosis* 60: 161-171.

39. Dean, W.R. 1928. The streamline motion of fluid in a curved pipe. *Philosophical Magazine* 7(5): 673-695.

40. Healthwise. Heart disease help center: Aortic aneurysm. WebMD, http://www.webmd.com/heart-disease/tc/aortic-aneurysm-overview (accessed March 8, 2010)

41. Mayo Clinic staff. Aortic Dissection. Mayo Clinic, http://www.mayoclinic .com/health/aortic-dissection/DS00605 (accessed March 8, 2010)

42. Healthwise. Heart disease help center: Aortic valve stenosis. WebMD, http://www.webmd.com/heart-disease/tc/aortic-valve-stenosis-overview (accessed March 8, 2010)

43. National Organization of Rare Disorders. Heart disease help center: Endocarditis, infective. http://www.webmd.com/heart-disease/endocarditis-infective (accessed March 8, 2010).